THE JOURNAL OF BIOLOGICAL CHEMISTRY VOL. 286, NO. 2, pp. 1517–1527, January 14, 2011

Cellular and Molecular Mechanisms of Autosomal Dominant Form of Progressive Hearing Loss, DFNA2*[S]

Received for publication, August 26, 2010, and in revised form, October 2, 2010 Published, JBC Papers in Press, October 21, 2010, DOI 10.1074/jbc.M110.179010

Hyo Jeong Kim, Ping Lv, Choong-Ryoul Sihn, and Ebenezer N. Yamoah[1]

From the Department of Anesthesiology and Pain Medicine, Program in Communication Science, School of Medicine, University of California, Davis, California 95618

Despite advances in identifying deafness genes, determination of the underlying cellular and functional mechanisms for auditory diseases remains a challenge. Mutations of the human K^+ channel hKv7.4 lead to post-lingual progressive hearing loss (DFNA2), which affects world-wide population with diverse racial backgrounds. Here, we have generated the spectrum of point mutations in the hKv7.4 that have been identified as diseased mutants. We report that expression of five point mutations in the pore region, namely L274H, W276S, L281S, G285C, and G296S, as well as the C-terminal mutant G321S in the heterologous expression system, yielded non-functional channels because of endoplasmic reticulum retention of the mutant channels. We mimicked the dominant diseased conditions by co-expressing the wild-type and mutant channels. As compared with expression of wild-type channel alone, the blend of wild-type and mutant channel subunits resulted in reduced currents. Moreover, the combinatorial ratios of wild type:mutant and the ensuing current magnitude could not be explained by the predictions of a tetrameric channel and a dominant negative effect of the mutant subunits. The results can be explained by the dependence of cell surface expression of the mutant on the wild-type subunit. Surprisingly, a transmembrane mutation F182L, which has been identified in a pre-lingual progressive hearing loss patient in Taiwan, yielded cell surface expression and functional features that were similar to that of the wild type, suggesting that this mutation may represent redundant polymorphism. Collectively, these findings provide traces of the cellular mechanisms for DFNA2.

The importance of K^+ channels in controlling the membrane properties of excitable and non-excitable cells is underpinned by the plethora of genetic diseases that ensue from mutations of genes encoding these channels (1–5). For example, in the inner ear, Kv7 (KCNQ) channels are expressed abundantly in inner/outer hair cells and spiral ganglion neurons, and the current serves as one of the essential determinants of the resting membrane potential (V_{rest}) (6–8). Additionally, activation of Kv7 channel currents may promote K^+ recycling between the perilymph and the K^+-rich endolymph, establishing dynamic flux of ions across the membranes of sensory and non-sensory cells of the cochlear duct (9, 10). Moreover, at the lateral wall of the cochlear duct, the cytoarchitecture of non-sensory cells and the rapid flux of ions favor the generation of an extracellular field potential of ~80 mV that defines the cochlear duct as the hub of "the battery" of auditory transduction (11, 12). Accordingly, mutations or null deletions of *Kv7.4* in humans and animal models result in gradual degeneration of hair cells and spiral ganglion neurons, described as an autosomal dominant form of non-syndromic progressive hearing loss (DFNA2) (13–15). Although the coarse features of Kv7.4 channel functions in the auditory system have been identified, the cellular and functional mechanisms of the mutant channels in DFNA2 remain unknown despite its global implication.

DFNA2 affects families of diverse backgrounds ranging from Europeans and American families to families of Asian origins. In humans, *Kv7.4* is located on chromosome 1p34 (16, 17). To date, as many as eight missense mutations have been reported resulting in seven specific point mutations, and in two extreme cases, there are frameshift mutations that end up with small truncated peptides (see Table 1). Moreover, a substantial number of the missense mutations, six out of eight, have been identified in the pore (P)-loop of Kv7.4 channels, including the GYG K^+ filter region. The remaining two missense mutations are located at S3 and the C-terminal domains. Only two mutant forms, G285S and G296S, have been evaluated at the cellular level to determine the functional implications in heterologous expression system (2, 18).

To address the underlying cellular and functional mechanisms of DFNA2, we generated seven mutant forms of the human Kv7.4 clone using site-directed mutagenesis. We then defined their subcellular localization and tested their electrophysiological properties. The pore mutations of the channels resulted in non-functional channels. Additionally, the pore mutant channels had defective channel trafficking and cell surface expression. Moreover, the C-terminal mutation G321S produced similar dual effects. In contrast, the S3 mutation had functional phenotypes that were similar to the wild-type channel, yielding an unexpected finding that may represent polymorphism, and requiring further investigation. Thus, this report provides cellular and molecular mechanisms of Kv7.4 function for DFNA2.

* This work was supported, in whole or in part, by National Institutes of Health Grants through DC010386 and DC007592 the NIDCD (to E. N. Y.).
[S] The on-line version of this article (available at http://www.jbc.org) contains supplemental Figs. S1–S4.
[1] To whom correspondence should be addressed: Dept. of Anesthesiology and Pain Medicine, Program in Communication Science, School of Medicine, University of California, 1515 Newton Ct., Davis, CA 95618. Fax: 530-754-7183; E-mail: enyamoah@ucdavis.edu.

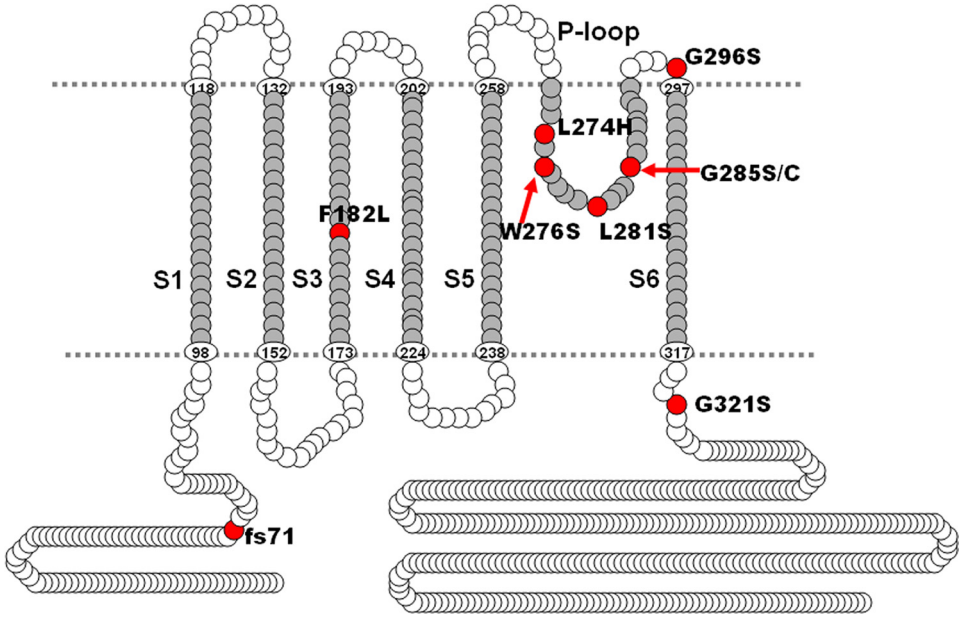

FIGURE 1. **Schematic representation of hKv7.4 protein structure.** Known mutations are indicated as *red circles*. Amino acid numbers in six transmembrane domains S1–S6 and the pore region were based on UniProtKB/Swiss-Prot P56696.

TABLE 1
KCNQ4 mutations in DFNA2 families

Family	Amino acid change	DNA change	Protein domain	Exon	Ref.
French	G285S	G853A	Pore region	6	(2)
American I	G285C	G853T	Pore region	6	(40)
Belgian	Fs71X134	211del13	N-terminal cytoplasmic	1	(40)
Dutch I	W276S	G827C	Pore region	5	(40)
Japanese I					(41)
Japanese II					(3)
Dutch IV					(3)
Dutch V					(26)
Dutch II	G321S	G961A	C-terminal cytoplasmic	7	(40)
American II	L281S	T842C	Pore region	6	(25)
Dutch III	L274H	T821A	Pore region	5	(42)
Japanese III	Fs71X138	211del1	N-terminal cytoplasmic	1	(43)
Taiwanese	F182L	C546G	S3 transmembrane	4	(23)
Spanish	G296S	G886A	Pore region	6	(18)

EXPERIMENTAL PROCEDURES

Ethical Approval—All procedures in this report were approved by the Institutional Animal Care and Use Committee of University of California, Davis, CA.

Generation of Mutant Forms of hKv7.4 and Epitope-tagged Construct—Wild-type (WT) hKv7.4 clones, isoform a, 695 amino acids (gene ID: NM_004700) and isoform b, 641 amino acids (gene ID: NM_172163), were purchased from Qiagen (Valencia, CA). The CDS were subcloned into pIRES2-EGFP plasmid vector (Clontech). Seven missense mutations were generated from wild-type gene using the QuikChange II mutagenesis kit (Stratagene, La Jolla, CA) and verified by automated sequencing. pIRES2-EGFP-hKv7.4-WT and mutants were used in an electrophysiology/patch clamp study using EGFP expression as a transfection marker. For the study of subcellular localization of WT and mutant (MT)[2] subunits, two different epitopes, modified HA- and c-Myc tags, were inserted into pCMV-hKv7.4-WT and mutant constructs in which EGFP genes were eliminated. Modified HA- and c-Myc epitopes were flanked with ClC-5 chloride channel D1–D2 loop to increase accessibility and inserted in the end of the S1–S2 loop of hKv7.4 as described previously in Kv7.2/7.3 (19) and Kv7.4 (18) channels. S1–S2 loop amino acid sequences were changed to STIQEHQELANENSEH**YPYDVPDYA**VTFEERDKCPEWNC for HA-tagged constructs and STIQEHQELANENSEH**EQKLISEEDL**VTFEERDKCPEWNC for c-Myc tagged constructs; whole inserted regions are underlined, and epitopes are shown in bold. Epitope tags were generated by recombination polymerase chain reaction and verified by automated sequencing.

Cell Culture and hKv7.4 Gene Delivery—Chinese hamster ovary (CHO) cell line was maintained in F-12 media with 10% fetal bovine serum (FBS) and 1× antibiotic-antimycotic mixture (Invitrogen) at 37 °C with 5% CO_2. Cells were seeded onto 12-mm coverslips in F-12 + 10% FBS without antibiotics and cultured 12–24 h before transfection. hKv7.4-WT or hKv7.4 mutant DNA was transiently transfected into cells singly or in combinations, at a total amount of 200 ng/well, using Lipofectamine 2000 (Invitrogen) according to the manufacturer's instructions.

[2] The abbreviations used are: MT, mutant; ER, endoplasmic reticulum; DN, dominant negative; NP, non-permeabilized; F, Farads.

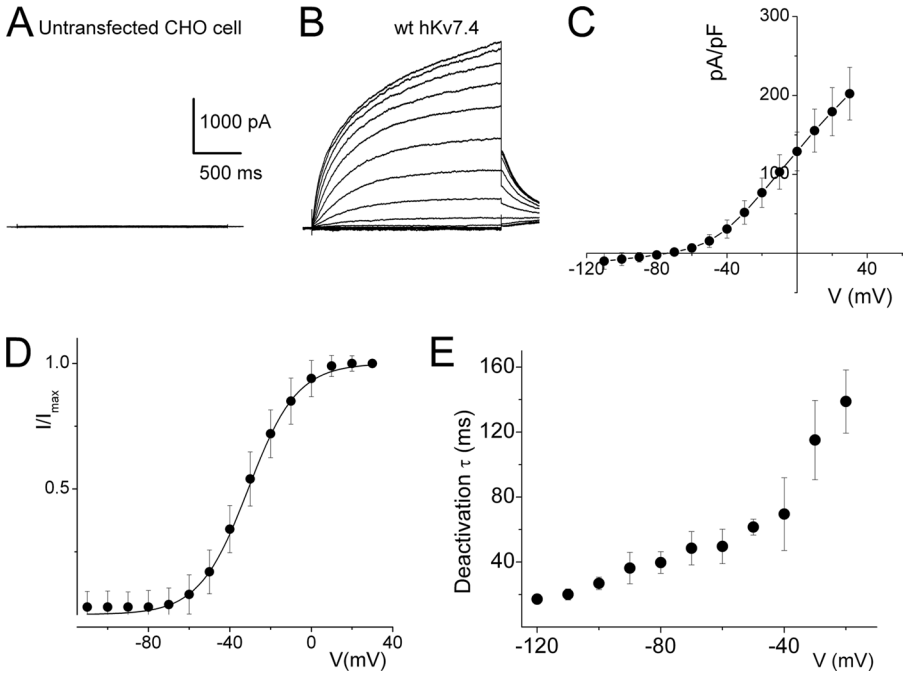

FIGURE 2. **Whole-cell K^+ currents derived from hKv7.4 channels in CHO cells.** *A*, untransfected and GFP alone-transfected CHO cells did not yield measurable current. Shown are examples of current traces recorded from CHO cells that were transfected with GFP alone. CHO cells were held at −80 mV, and the step voltages ranged from −110 to 40 mV at 10-mV increments. *B*, membrane K^+ currents traces recorded from CHO cells after 24 h of transfection with hKv7.4, at a holding potential of −80 mV and with step voltages ranging from −110 mV to 40 mV, with $\Delta V = 10$ mV. Non-transfected cells did not yield measurable current (data not shown). *C*, the corresponding current density-voltage relation shown was generated from $n = 27$ cells. The activation voltage of the expressed hKv7.4 current was ~−60 mV. *D*, voltage dependence of steady-state activation generated from tail currents (I) as a ratio of the maximum tail current (I_{max}). Each symbol represents the mean current ratio obtained from 17 cells. The *continuous line* represents a single Boltzmann function fit to the data points. The half-activation voltage ($V_{1/2}$) was −31 ± 1 mV, and the slope was e-fold for 11 ± 0.5 mV ($n = 17$). *E*, deactivation of the current as a function of voltage ranged from 17 ± 3 ms at −120 mV to 139 ± 20 ms ($n = 15$) at −20 mV.

Electrophysiological Recordings—Whole-cell voltage clamp recordings were performed from single, uncoupled cells at room temperature (20–22 °C) using an Axopatch 200A amplifier (Axon Instruments, Inc. Union City, CA). Fire-polished electrodes (3–4 megaohms) were pulled from borosilicate glass. The electrodes contained (in mM): 140 KCl, 1 $MgCl_2$, 10 HEPES, 10 EGTA, 1 CaCl, 4 K_2ATP, pH 7.2, with KOH. The external bathing solution was constantly perfused (2–3 ml/min) and contained (in mM): 145 NaCl, 4 KCl, 1.8 $CaCl_2$, 0.5 $MgCl_2$, 10 HEPES, 5 D-glucose, pH 7.4, with NaOH. Outward hKv7.4 channel current traces were generated with depolarizing voltage steps from a holding potential of −80 mV and stepped to varying step potentials ($\Delta V = 10$ mV). Currents were measured after capacitance compensation and series resistance compensation (6–8 megaohms) (nominally 70–90%), filtered at 2 kHz using an 8-pole Bessel filter, and sampled at 5 kHz. Liquid junction potentials were less than 2 mV (1.4 ± 0.3 mV, $n = 11$). Whole cell K^+ current amplitude at varying test potentials was measured at steady-state levels using a steady-state detection routine; the current was divided by the cell capacitance (pF) to generate the current density-voltage relationship. Analyses of data were performed using custom-made software and MicroCal Origin (Northampton, MA) programs. Pooled data are presented as means ± S.D. Multiple comparisons *versus* control data were performed using *t* test or Kruskal-Wallis one-way analysis of variance (Dunn's method). Whole-cell K^+ currents were normalized and plotted against the step potential. Continuous curves

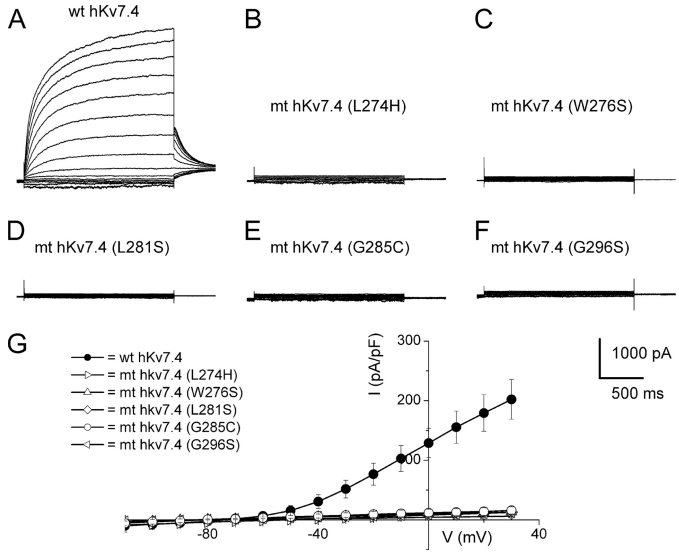

FIGURE 3. **Pore mutants of hKv7.4 channels did not produce measurable currents.** *A*, characteristic WT current traces recorded from a holding potential of −80 mV and activated from −110 mV to 30 mV with ΔV of 10 mV as described in the legend for Fig. 2. *B–F*, using similar activation voltage steps as described in *A*, CHO cells transfected with hKv7.4 MT channels, with point mutations at the pore region of the channel, namely L274H (*B*), W276S (*C*), L281S (*D*), G285C (*E*), and G296S (*F*), were assessed. None of the pore region mutants yielded detectable current. *G*, current density (in pA/pF)-voltage relations of the wild-type and mutant channels. Each data set designated with symbols shown represents the mean of 15 cells.

were generated from the Boltzmann function $I/I_{max} = (1 + (\exp(V_{1/2} - V)/k_m))$, where $V_{1/2}$ is the half-activation voltage, $k_m = RT/zF$ is the slope factor, I is the magnitude of the cur-

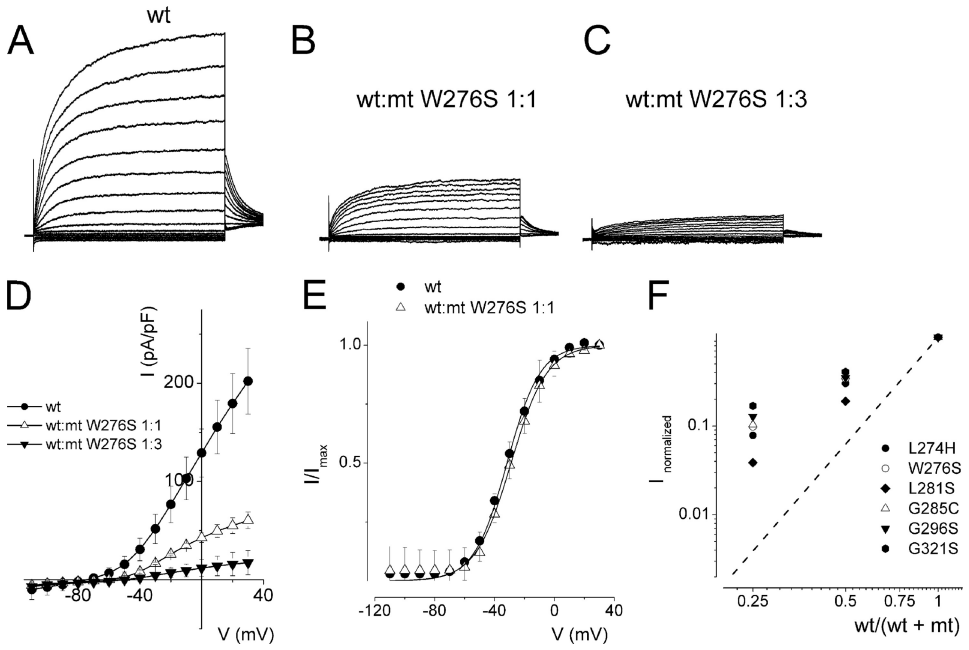

FIGURE 4. **Activation properties of heteromeric hKv7.4 channel currents.** Whole-cell outward currents were recorded upon expressing the WT channel singly (*A*) and co-expressing WT hKv7.4 and MT W276S at a ratio of 1:1 (*B*). *B*, representative current traces for a family of K^+ currents obtained from a holding potential of −80 mV and stepped from −110 to 40 mV using $\Delta V = 10$ mV are shown. The tail currents were elicited at −40 mV. *C*, current traces recorded from CHO cells transfected with a WT:MT ratio of 1:3. *D*, plots of current density-voltage relation of currents derived from WT hKv7.4 alone (●) and a combination of WT Kv7.4 and MT W276S (1:1, △, and 1:3, ▼). The current density (pA/pF) at a step potential of 30 mV for WT hKv7.4 was 202 ± 33, as compared with the combined WT:MT W276S (1:1) ratio, which was 60 ± 8, and the WT:MT W276S (1:3) ratio was 17 ± 13 ($n = 11$; $p < 0.05$). *E*, the effects of MT W276S on WT-hKv7.4 currents did not alter the gating properties. Steady-state activation curves of WT Kv7.4 alone (●) and after suppression by MT-W276S (△, ratio 1:1) are shown. Tail currents were measured immediately after pulsing to −40 mV, normalized to the largest tail recorded, and plotted against the preceding prepulse voltages. Neither the midpoint ($V_{1/2}$, in mV) nor the slope factors (*k*, in mV) were statistically different among the two groups. The $V_{1/2}$ and *k* values for WT Kv7.4 alone were: −32 ± 2 and 11.9 ± 1. The $V_{1/2}$ and *k* values for WT Kv7.4:MT W276S (1:1) were: −29 ± 2 and 11.9 ± 0.5 mV ($n = 11$; $p = 0.3$ and 0.4). *F*, current suppression of WT Kv7.4 by MT channels, L274H (●), W276S (○), L281S (◆), G285C (△) G296S (▼), and G321S (□) *versus* WT/(WT + MT) ratio of DNA transfected. Suppression of hKv7.4 currents increased with decreasing WT:MT ratio. *Dashed lines* denote the predicted suppression ratio expected for tetrameric channel. The experimental data deviated from the predicted relationship of tetrameric K^+ channel (see "Discussion").

rent, and I_{max} denotes the maximum current magnitude. Assuming that K^+ channel monomers assemble to form a conducting pore and because stoichiometric combination of the WT and mutant monomers should be stochastic, the probability of forming a functional channel with only WT monomers ($P_{WT\ only}$) can be described by a polynomial distribution with the proportion of WT monomers (p_{WT}) available to the *n*th power ($P_{WT\ only} = p_{WT}{}^n$), where *n* is the number of monomers present in a channel (20).

Immunostaining—The primary antibodies used were: mouse monoclonal anti-hKv7.4 (NeuroMab, Davis, CA), mouse monoclonal anti-HA (Covance, Emeryville, CA), rabbit polyclonal anti-HA, chicken polyclonal anti-c-Myc, rabbit polyclonal anti-cytochrome P450 (Abcam, Cambridge, MA), mouse monoclonal anti-early endosome antigen 1 (EEA1), mouse monoclonal anti-golgin A4 (P230), and mouse monoclonal anti-golgin A2 (Golgi matrix protein of 130 kDa) (BD Biosciences) in 1 μg/ml final concentration. The secondary antibodies were: donkey anti-mouse-Cy3, donkey anti-mouse-Cy5, donkey anti-rabbit-Cy3, donkey anti-rabbit-Cy5, and donkey anti-chicken-Cy5 (Jackson ImmunoResearch Laboratories, West Grove, PA) in the manufacturer's recommended concentrations. CHO cells were incubated 24 h after transfection and fixed in 4% paraformaldehyde in 1× phosphate-buffered saline (PBS) for 10 min followed by PBS washing. To use anti-hKv7.4 antibody and to study intracellular localization, cells were permeabilized and blocked in 0.1% Triton X-100, 3% bovine serum albumin (BSA), and 5% normal donkey serum in PBS for 30 min at 37 °C. For plasma membrane staining against HA and c-Myc tags, cells were blocked in 3% BSA and 5% normal donkey serum in 1× PBS without Triton X-100 permeabilization. Cells were incubated in primary antibodies at 4 °C overnight, washed with chilled (4°C) PBS three times, and incubated in secondary antibodies at room temperature for 90 min followed by 5 min of DAPI staining with PBS washing. Slides were mounted with ProLong Gold mounting medium (Invitrogen), and images were taken using confocal microscope (Carl Zeiss, LSM510). Unless indicated otherwise, reagents were obtained from Sigma-Aldrich.

TABLE 2

Activation and deactivation kinetics of hKv7.4/mt channels

Data for the individual activation and deactivation time constants from CHO cells expressing of wild type and each mutant with 1:1 ratio were obtained from five to seven cells. All values are mean ± S.D. (*, $p < 0.05$, **, $p < 0.01$).

	$\tau_{activation}$ (40 mV)		$\tau_{deactivation}$ (−40 mV), τ (ms)
	τ_{fast} (ms)	τ_{slow} (ms)	
WT	107 ± 14	698 ± 71	178 ± 38
F182L	83 ± 21*	587 ± 90*	111 ± 48
WT:F182L	91 ± 19*	496 ± 81**	137 ± 16*
WT:L274H	114 ± 16	683 ± 28	158 ± 15
WT:W276S	174 ± 40**	629 ± 40*	142 ± 15
WT:L281S	87 ± 13**	466 ± 79**	110 ± 49
WT:G285S	85 ± 26	488 ± 87**	129 ± 28*
WT:G296S	75 ± 18**	458 ± 85**	121 ± 37*
WT:G321S	64 ± 14**	591 ± 81*	149 ± 32

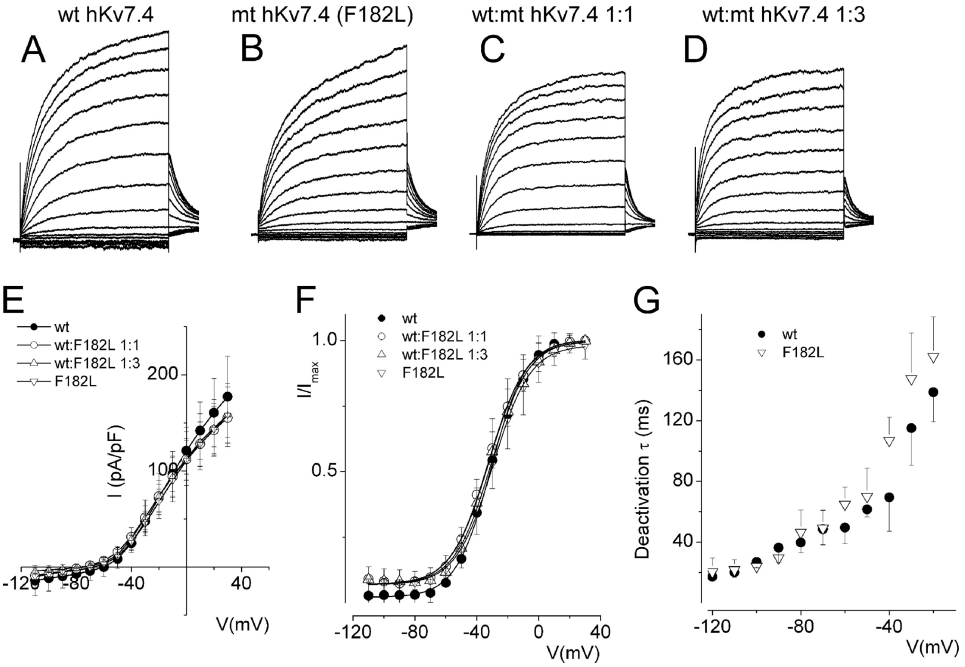

FIGURE 5. **Wild-type hKv7.4 and the transmembrane mutant F182L channels were expressed in CHO cells.** *A*, exemplary outward hKv7.4 current traces recorded from a holding potential of −80 to 30 mV using voltage increment of 10 mV in depolarizing and hyperpolarizing step voltages. *B–D*, current traces recorded from CHO cells, which were transfected with MT-F182L alone (*B*), WT-hKv7.4:MT-F182L (1:1) (*C*), and (1:3) (*D*). *E*, group data of current density-voltage curves (mean ± S.D.) for co-expression of WT-hKv7.4 alone (●) with WT-hKv7.4:MT-F182L (1:1, ○), (1:3, △), and (0:1,▽). *F*, summary data of the steady-state voltage-dependent activation of WT-hKv7.4 alone (●), WT:F182L (1:1, ○), (1:3, △), and (0:1, ▽). The $V_{1/2}$ of the steady-state activation curves of the four combinatorial expression and the ensuing currents were not statistically different. The $V_{1/2}$ (in mV) of WT-hKv7.4 alone and WT:F182L (1:1, 1:3, and 0:1 ratios) were −32.5 ± 0.5, −30.4 ± 1.0, −30.8 ± 0.7, and −32.1 ± 0.6, (n = 11, p = 0.3), respectively. The slope factors (k) of the resulting Boltzmann function curves were also not statistically different. The k values (in mV) of WT-hKv7.4 alone (●) and WT:F182L (1:1, 1:3, and 0:1 ratios) were 12.1 ± 0.5, 11.9 ± 0.8, 11.2 ± 1.0, and 12.0 ± 0.6 (n = 11; p = *0.2*), respectively. *G*, deactivation time constants (τ) of the current at −20 mV as a function of voltage for the wild-type and F182L channel currents are shown.

RESULTS

Mutations at multiple sites on the hKv7.4 channel have been identified to be associated with post-lingual high frequency-predominant hearing loss. The diversity of mutational sites and the heterogeneity of the hereditary disease coupled with varying symptoms ranging from early to late onset progressive hearing loss raise the possibility that the ensuing functional phenotypes of the mutant channels may differ. Shown in Fig. 1 is a graphical representation of the eight identified mutation sites (in *red*) at the transmembrane, pore loop, and C-terminal segments of the predicted hKv7.4 channel structure. Table 1 shows that one of the hKv7.4 mutations has been found across racial differences, suggesting that this site may represent a mutational hotspot (4). To determine the functional phenotypes of the known mutations, we first examined the properties of the WT hKv7.4 expressed in CHO cells, using green fluorescent protein (GFP) as a transfection marker. In contrast to untransfected and GFP alone-transfected CHO cells (Fig. 2*A*), hKv7.4-transfected cells yielded robust outward currents traces (Fig. 2*B*) in response to voltage steps ranging from −100 to 40 mV from a holding voltage of −80 mV. As is evident in Fig. 2, *C* and *D*, the activation voltage of hKv7.4 channel current was ~−60 mV, and the half-activation voltage ($V_{½}$) and the slope factor, k, derived from the Boltzmann function were (in mV); −31 ± 1 (n = 17) and 11.9 ± 0.5 (n = 17), respectively. The deactivation time constants (in ms) ranged from 17 ± 3 at −120 mV to 139 ± 20 at −20 mV (n = 15; Fig. 2*E*). Next, we compared differ-

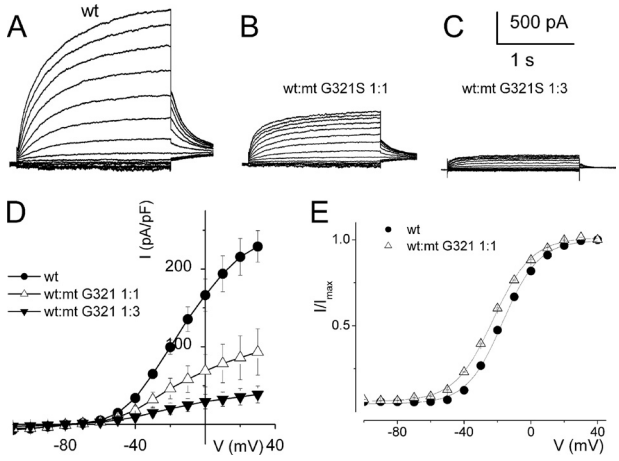

FIGURE 6. **Activation properties of heteromeric hKv7.4 channel and C-terminal mutant G321S currents.** *A*, whole-cell outward currents were recorded upon expressing the WT channel singly. *B*, current traces recorded after co-expressing WT hKv7.4 and MT G321S at a ratio of 1:1. Representative current traces for a family of K^+ currents obtained from a holding potential of −80 mV and stepped from −110 to 30 mV using ΔV = 10 mV are shown. The tail currents were elicited at −40 mV. *C*, current traces recorded from CHO cells transfected with a WT:MT-G321S ratio of 1:3. *D*, plots of current density-voltage relation of currents derived from WT hKv7.4 alone (●) and a combination of WT Kv7.4 and MT G321S (1:1, △, and 1:3, ▼). *E*, the effects of MT-G321S on WT-hKv7.4 currents did not alter the gating properties. Steady-state activation curves of WT Kv7.4 alone (●) and after suppression by MT-G321S (△, ratio 1:1) are shown. Tail currents were measured immediately after pulsing to −40 mV, normalized to the largest tail current recorded, and plotted against the preceding prepulse voltages. Neither the midpoint ($V_{1/2}$, in mV) nor the slope factors (k, in mV) were statistically different among the two groups. The $V_{1/2}$ and k for WT Kv7.4 alone and WT-Kv7.4:MT G321S were −31 ± 1, 11.8 ± 1, and −34 ± 3, and 11.9 ± 0.5 mV (n = 11; p = 0.5 and 0.6), respectively.

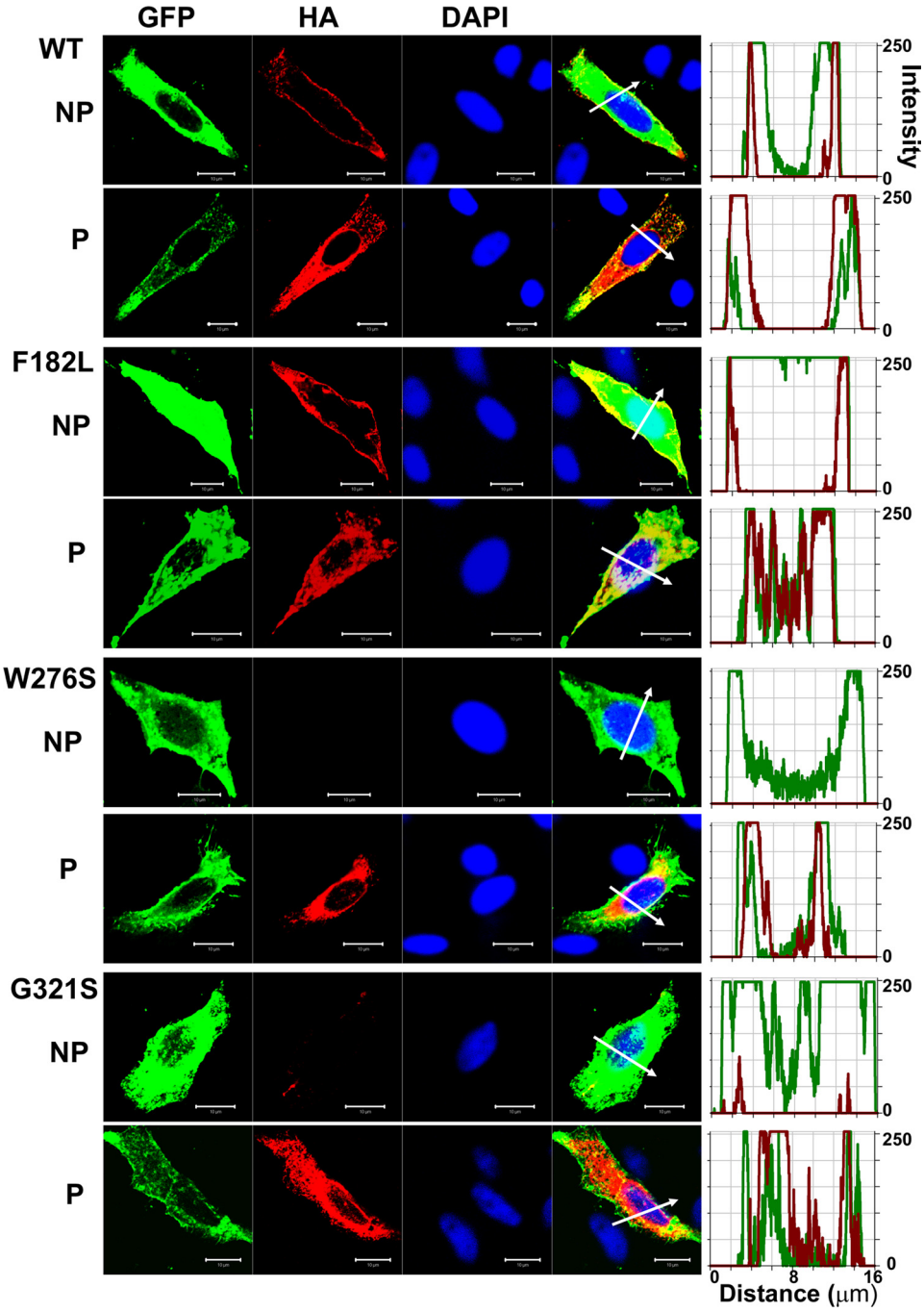

FIGURE 7. **Detection of cell surface expression of HA-tagged wild-type and mutant Kv7.4 channels.** HA epitope was inserted with an extension of ClC-5 chloride channel D1–D2 loop sequences into the Kv7.4 channel extracellular loop between the S1–S2 transmembrane domains. Farnesylated GFP was used as a reporter that binds to the plasma membrane. Anti-HA antibody stained only the Kv7.4 protein expressed in the cell surface in NP cells and stained both the cell surface and the cytoplasmically expressed protein in permeabilized cells (*P*). Fluorescent intensities of GFP (*green*) and the Kv7.4 channel (*red*) were plotted against the distance, which was marked in the merged image with the *white arrow*. The overlap of green and red signals in NP cells indicates the surface expression of Kv7.4 channels. The *scale bar* is 10 μm.

ences between the WT hKv7.4 current magnitude and outward current recorded from CHO cells transfected with pore mutants L274H, W276S, L281S, G285C, and G296S (Fig. 3). None of the pore mutants yielded measurable outward currents as compared with the WT hKv7.4 channel (Fig. 3, *A–G*).

K^+ channels consist of four pore-forming α-subunits (21). Mutations at the pore-forming region can cripple current conduction properties of the channel. The resulting dominant negative (DN) subunit, when co-assembled with the WT subunit, results in a non-functional channel (8). To examine whether the pore mutants were acting in a DN fashion, we transfected the WT and MT channel subunits singly, as seen in Fig. 3, and co-transfected the two channel subunits (WT and MT) at different ratios (WT:MT). Shown in Fig. 4, *A–C*, are the current traces recorded for WT:W276S ratios 1:0, 1:1, and 1:3. The corresponding current-density and voltage relationships are depicted in Fig. 4*D*. Comparing the WT (1:0) and WT:MT (1:1) currents, the steady-state voltage-depen-

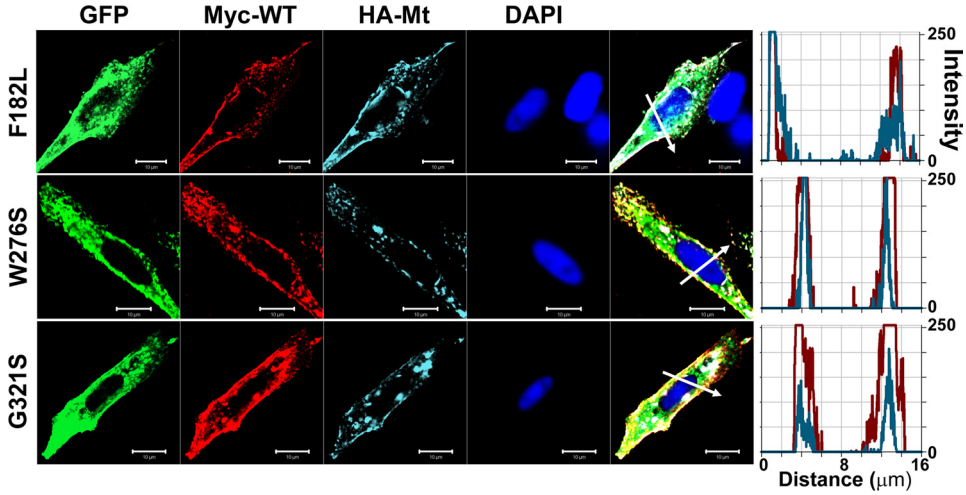

FIGURE 8. **Detection of cell surface expression of c-Myc-tagged wild-type and HA-tagged mutant Kv7.4 channels in co-expression.** c-Myc epitope was inserted into wild-type Kv7.4 as described for HA tag insertion. Farnesylated GFP was used as a reporter that binds to the plasma membrane. Anti-c-Myc and anti-HA antibodies double staining detected wild-type and mutant Kv7.4 protein, respectively, which were expressed on the cell surface, in non-permeabilized conditions. Fluorescent intensity of wild-type (*red*) and mutant (*cyan*) Kv7.4 channel were plotted against the distance, which was marked in the merged image with the *white arrow*. The overlap of red and cyan signals in NP cells indicates their co-localization on the cell surface. The *scale bar* is 10 μm.

dent activations fitted with a Boltzmann function were unaltered (in mV, WT, $V_{½} = -32 \pm 2$, $k = 11.9 \pm 1$ ($n = 11$); WT:MT (1:1), $V_{½}$, $= -29 \pm 2$, $k = 11.9 \pm 0.5$ ($n = 11$), $p = 0.3$) (Fig. 4*E*). Assuming the predicted tetrameric structure of K^+ channels (20), we calculated the expected current magnitude when the WT hKv7.4 channel is co-expressed with a DN mutant at different ratios. We have illustrated the expected results in Fig. 4*F* with a *dashed line*. The experimental data points (in symbols) for the pore mutants noticeably suggested that none of the mutant channels operated in a classical DN fashion (Fig. 4*F*). A straightforward but accurate mechanism to produce functional amputation of a channel is to accelerate the kinetics of deactivation (22). We examined the time constants (τ) of activation and tail currents produced by the wild-type and mixtures of wild-type and pore loop mutant channels (Table 2). The activation τ values were described by two components (fast and slow), and most of the pore mutants showed substantial changes in the τ values of activation. Additionally, the deactivation τ values were also altered in some mutants (Table 2).

Next, we examined mutations outside the pore of hKv7.4 channel that have been ascribed to DFNA2. Mutation F182L in the S3 transmembrane domain of hKv7.4 has been associated with profound pre-lingual deafness in a Taiwanese patient with non-syndromic deafness (23). To determine the cellular mechanisms of the disease, we expressed F182L singly and at different ratios with the WT subunit. CHO cells transfected with F182L mutant DNA yielded robust current that was visibly similar to the wild-type channel current in terms of both magnitude and kinetics (Fig. 5, *A–G*). Additionally, transfection with mixtures of F182L and the WT DNA produced currents with comparable magnitudes (Fig. 5, *C–E*), voltage-dependent activation properties, and deactivation time constants (Fig. 5, *F* and *G*).

A site at the C-terminal of the hKv7.4 channel has also been identified in a Dutch family that bears the mutation G321S, which is thought to be the underlying etiology for the post-lingual progressive non-syndromic hearing loss in these patients (16). CHO cells transfected with the G321S mutant DNA yielded no measurable current as compared with the WT channel (data not shown). Co-transfection of the G321S and the WT DNA at different ratios produced sizable currents, which were smaller in magnitude as compared with CHO cells transfected with the WT channel alone (Fig. 6, *A–D*). The voltage-dependent activation properties (Fig. 6*E*) and deactivation kinetics of the WT:G321S 1:1 mixture (Table 2) and WT alone currents were not substantially different. However, activation kinetics were significantly different (Table 2).

An important assumption that is implicit in the analysis performed and described in Fig. 4*F* regarding the predicted current magnitude after co-transfection of MT hKv7.4 and the WT DNA is that the two subunits are synthesized and trafficked independently and then assembled in equivalent ratiometric proportions at the plasmalemma (8, 20). Any tilt in the scales of the aforementioned processes should result in deviations from the predicted results, as demonstrated (Fig. 4*F*). To understand the cellular mechanisms that explain why MT-hKv7.4 channel expressed in CHO cells did not yield current (Figs. 2–3), we determined the cell surface expression of Kv7.4 channels. To detect cell surface expression of wild-type and MT-hKv7.4 channels, we used HA and c-Myc epitope tags in the extracellular loop between S1–S2 transmembrane domains. Farnesylated GFP was used as reporter for the plasma membrane. HA- and c-Myc-tagged hKv7.4 channels yielded currents that were similar to the untagged channels (supplemental Fig. S1). As shown in supplemental Fig. S2, HA- and c-Myc-tagged wild-type hKv7.4 channels were labeled mainly in the plasma membrane in non-permeabilized (NP) cells as compared with Kv7.4 antibody labeling directed against the intracellular N-terminal of the channel, which did not show positive reactivity in NP con-

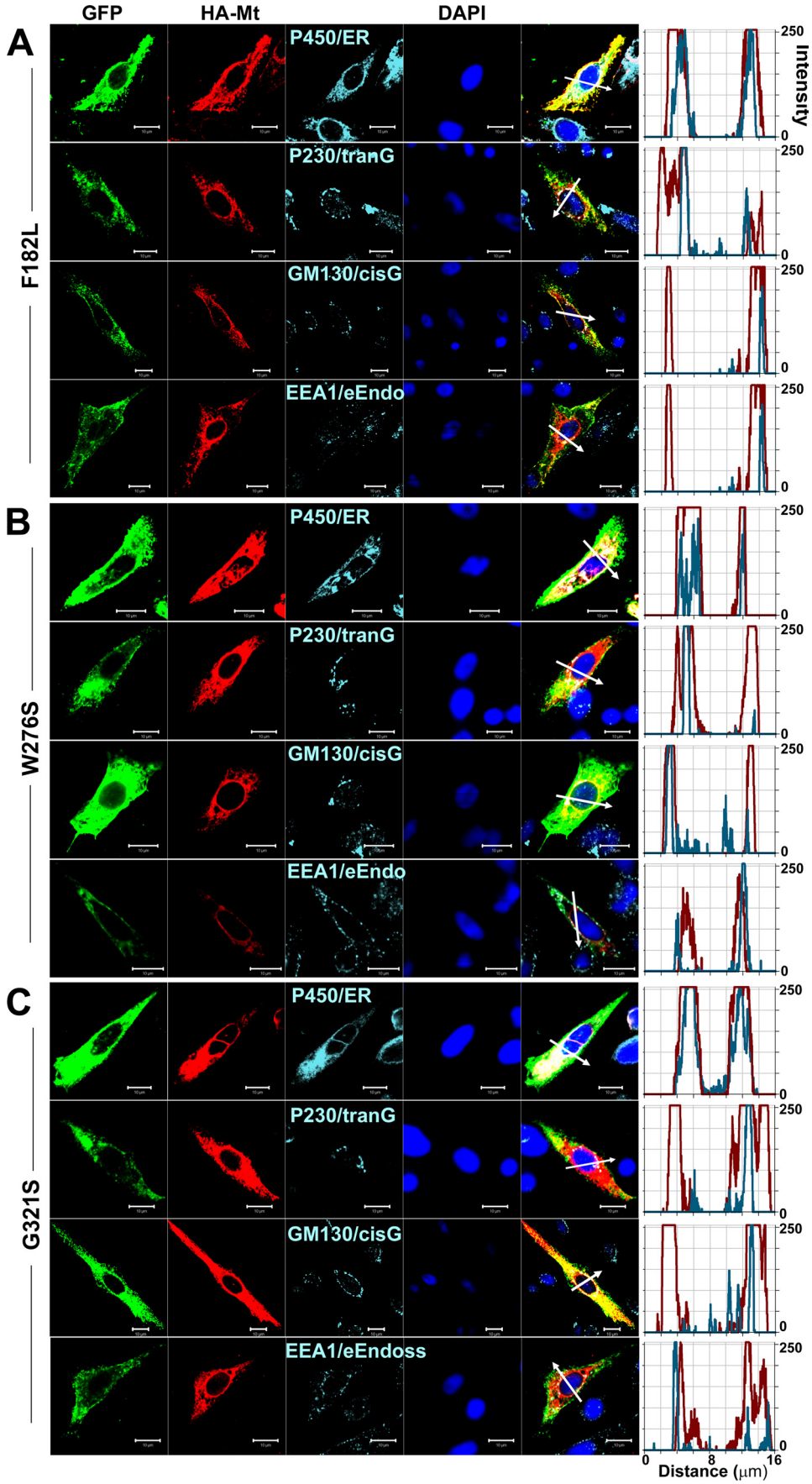
GFP
HA-Mt
DAPI
A
F182L
P450/ER
P230/tranG
GM130/cisG
EEA1/eEndo
B
W276S
P450/ER
P230/tranG
GM130/cisG
EEA1/eEndo
C
G321S
P450/ER
P230/tranG
GM130/cisG
EEA1/eEndoss
250
0
Intensity
0
8
16
Distance (μm)

ditions. In keeping with the functional data, and as demonstrated in Fig. 7, the wild-type and F182L channels were synthesized, trafficked, and localized robustly in the plasma membrane. Moreover, the pore mutant W276S and the C-terminal mutant G321S were synthesized but not localized in the plasma membrane, suggesting that these MT channels had impaired trafficking mechanisms (Fig. 7). Indeed, all of the pore mutants, L274H, L281S, G285C, and G296S, did not show plasma membrane localization when expressed singly (supplemental Fig. S3), indicating defective membrane trafficking. However, under dominant gene diseased conditions, the WT gene product is expected to be synthesized together with the MT subunit in heterozygote patients. Thus, we determined whether the expression of the WT subunit may facilitate mutant-subunit trafficking by co-expressing c-Myc-tagged WT and HA-tagged MT subunits in CHO cells. In contrast to the lack of mutant channel trafficking when expressed alone (Fig. 7 and supplemental Fig. S3), we demonstrated that expression of the MT subunits in conjunction with the WT subunit promotes trafficking and plasma membrane localization of the MT channels W276S and G321S (Fig. 8). Similarly, co-expression of the WT subunit with the mutants L274H, L281S, G285C, and G296S resulted in membrane localization of the mutant channels (supplemental Fig. S4).

Finally, we determined the subcellular organelle retention of HA-tagged mutant hKv7.4 channels in permeabilized CHO cells using anti-cytochrome P450 as endoplasmic reticulum (ER), anti-golgin A4 (P230) as trans-Golgi, anti-golgin A2 (GM130) as cis-Golgi, and anti-early endosome antigen 1 (EEA1) as endosome markers. Invariably, a substantial portion of the expressed mutant channels was identified mainly in the ER. Using the reported transmembrane mutant F182L, pore mutant W276S, and the C-terminal mutant G321S as examples, we show that the non-functional mutant channels are retained largely in the ER (Fig. 9). Thus, our analyses of the functional and cellular mechanisms of the reported mutations of hKv7.4 channel have revealed surprising, yet intricate, results that cannot be explained solely by the heteromeric interaction between the wild-type and mutant channels in the diseased conditions.

DISCUSSION

In this report, we have confirmed impaired cell surface expression of the pore segment mutation G296S of hKv7.4 (18) and have demonstrated that all known pore region mutations of the channel that have been reported to cause progressive hearing loss in humans (L274H, W276S, L281S, and G285C) exhibit similar expression phenotype. Functionally, none of the pore segment mutants yielded measurable current. Moreover, co-expression of the pore segment mutants with the wild-type subunits facilitates plasma membrane expression of the mutant channels, suggesting that the expected dominant diseased conditions may be complicated by unequal and interdependent trafficking of the two-channel subunits. The ensuing membrane current cannot be explained simply by predictions of independent heteromultimerization of the wild-type and mutant channels and/or by the DN effect of the mutant. Thus, the dependence of cell surface expression of the mutant on wild-type channels is the likely explanation for the deviation from the expected current magnitude using the analyses described in Fig. 4*F*. The C-terminal mutant G321S had expression phenotype that was similar to the pore region mutants. We also explored the possibility that a mechanism that can amputate a channel would be to accelerate the kinetics of deactivation (22). Although in some cases of WT:MT co-expression (Table 2), the deactivation time constants were abbreviated, the changes were modest, making it an unlikely mechanism to be the underlying cause for the disease. Cell organelle retention of the mutant channels occurs mainly at the level of the ER, suggesting that pore and C-terminal mutations of hKv7.4 constitute ER retention (24). On the contrary, the plasma membrane expression and electrophysiological phenotype of the transmembrane mutant F182L were similar to wild-type channels (23), raising the possibility that the identified mutation may not be responsible for the non-syndromic deafness associated with the reported patient. From this foothold, this report has probed the underlying cellular and functional mechanisms for the non-syndromic progressive hearing loss associated with mutations of the hKv7.4 channel.

Mutations of *hKv7.4* have global impact. The locus for DFNA2 was originally linked to chromosome 1 by linkage analysis in Indonesian, American, and Dutch families with progressive hearing impairment (16) and localized to the 1p34 region by analysis in a Belgian family and two Dutch families (17). Subsequent to the cloning of the *$hK_V7.4$* gene and mapping to 1p34 (2), mutant screenings of autosomal dominant progressive hearing loss patients, without linkage analysis, have identified mutations in European, American, Japanese, and Taiwanese families (Table 1).

Typically, the symptoms of DFNA2 patients from different families are similar through generations but not identical. Deafness develops slowly over decades, is post-lingual, and is presented as a symmetrical impairment. The disease begins as loss of high frequency hearing and progresses to middle and low frequencies within the next decade, without vestibular defect (4, 8). Moreover, the symptoms are not identical among these families, such as the age of onset and the presence of tinnitus. For example, in most patients, the onset of symptoms ranged from 5 to 15 years old, developing to severe hearing loss by ~50 years old. Although tinnitus was not reported in Dutch, Japanese, and Spanish families having

FIGURE 9. **Detection of subcellular localization of mutant Kv7.4 channels.** HA-tagged mutant Kv7.4 channels and subcellular organelles were double-stained in permeabilized cells s follows: *P450/ER*, anti-cytochrome P450 as endoplasmic reticulum marker; *P230/tranG*, anti-golgin A4 (P230) as trans-Golgi marker; *GM130/cisG*, anti-golgin A2 (Golgi matrix protein of 130 kDa) as cis-Golgi marker; *EEA1/e-Endo*, anti-early endosome antigen 1 as endosome marker. Fluorescent intensities of mutant Kv7.4 (*red*) and subcellular organelles (*cyan*) were plotted against the distance, which was marked in a merged image with a *white arrow*. The overlap pattern of red and cyan signals showed different levels of co-localization between organelles. *A–C*, F182L (*A*), W276S (*B*), and G321S (*C*) mutant channels. The *scale bar* is 10 μm.

W276S, G321S, and G296S mutations, in one American family with ancestors from France and Luxembourg, patients with the G285C mutation have profound hearing loss by the age of 40 with severe tinnitus (16). Meanwhile, in another American family with Austrian ancestry and having the L281S mutation, hearing loss was reported as early as age 3, high frequency hearing loss was diagnosed by age 6, and profound tinnitus was reported in most patients (25). W276S mutations were found in multiple families, but it was shown that these families did not have similar genetic background by microsatellite analysis and intragenic single nucleotide polymorphism methods (3, 26).

Unlike the pore region and C-terminal mutations found in 3–5 generations of families around the world with post-lingual hearing loss, the transmembrane segment mutation F182L has been identified in only one patient with pre-lingual profound deafness in a mutation screening of a non-syndromic deaf patient in Taiwan (23). Moreover, no other family member of the Taiwanese patient was identified to have hearing loss. Along with the similar electrophysiological features and cell surface localization of the F182L mutant channel, the apparent F182L mutation may not be responsible for the reported non-syndromic deafness of the patient but rather the result of polymorphism, as seen in *KCNE* in Caucasian population with Ménière disease (27). Thus, the hearing loss in the F182L mutant patient may ensue from an unknown etiological mechanism of deafness that requires further investigations.

Although the cellular and functional mechanisms of the pore segment and C-terminal mutants of hKv7.4 are to a rough approximation similar, differences in age of onset and symptoms of DFNA2 patients endure. The M-current, the phenotypic current derived from Kv7 channels, dictates the resting potential of hair cells and spiral ganglion neurons (7), and it is expected that reduction in the current magnitude in disease conditions will confer membrane depolarization, resulting in increased excess intracellular Ca^{2+} and Ca^{2+}-induced cell death (6, 7, 28). The progressive nature of the disease may reflect age-induced reduction in expression of the channels. However, the properties of the native M-current in hair cells and spiral ganglia neurons may be obscured by the findings that the current is regulated not only by the promiscuous interaction of Kv7.2–5 channels (8) but also by their accessory subunits KCNEs and by interaction with Kv11 channels (29–32). Thus, results determined from CHO cells may differ from the properties of channels expressed in hair cells and neurons. It is also conceivable that differences in disease onset and symptoms may ensue from the association of the mutant channels and their accessory subunits.

Another disposing factor that may precipitate different symptomatic outcomes of the disease is exposure to legitimate drugs that have pharmacological impact on hKv7.4 channels. For example, salicylate, one of the most commonly used non-steroidal anti-inflammatory drugs in the world, has a side effect of inducing temporary hearing loss and tinnitus (33, 34). Although previous studies have implicated salicylate-induced tinnitus to the drug-mediated increased cochlear arachidonic acid level and subsequent enhancement of *N*-methyl-D-aspartate receptor responses to glutamate (35, 36), other studies have attributed the cellular mechanisms of salicylate to impaired sound amplification by outer hair cells through salicylate action on electromotility (37–39). Moreover, salicylate concentrations required to mimic these effects are not in keeping with the serum salicylate concentrations (34). Recently, it has been demonstrated that the physiological target for salicylate-induced ototoxicity is the Kv7 channels (33). Thus, variable exposure to salicylate by DFNA2 patients may dictate the onset of the disease.

Previous studies have demonstrated that expression of G285S in heterologous expression systems yielded no measurable current (2, 8). Meanwhile, co-expression of the wild-type and the mutant subunits at different ratios produced current magnitudes, which were in keeping with the G285S serving as a DN mutant (2, 8). Here, it appears that replacement of serine to cysteine at the pore region of hKv7.4 alters channel trafficking and plasma membrane expression. It is conceivable that upon cell surface expression, the G285C mutant may produce a DN effect on the wild-type channel. Moreover, the results point to the intricate and complex mechanisms involved in the etiology of DFNA2.

Acknowledgments—We thank members of our laboratory for constructive comments.

REFERENCES

1. Cooper, E. C. (2001) *Epilepsia* **42,** Suppl. 5, 49–54
2. Kubisch, C., Schroeder, B. C., Friedrich, T., Lütjohann, B., El-Amraoui, A., Marlin, S., Petit, C., and Jentsch, T. J. (1999) *Cell* **96,** 437–446
3. Van Camp, G., Coucke, P. J., Akita, J., Fransen, E., Abe, S., De Leenheer, E. M., Huygen, P. L., Cremers, C. W., and Usami, S. (2002) *Hum. Mutat.* **20,** 15–19
4. Jentsch, T. J. (2000) *Nat. Rev. Neurosci.* **1,** 21–30
5. Casimiro, M. C., Knollmann, B. C., Yamoah, E. N., Nie, L., Vary, J. C., Jr., Sirenko, S. G., Greene, A. E., Grinberg, A., Huang, S. P., Ebert, S. N., and Pfeifer, K. (2004) *Genomics* **84,** 555–564
6. Holt, J. R., Stauffer, E. A., Abraham, D., and Géléoc, G. S. (2007) *J. Neurosci.* **27,** 8940–8951
7. Oliver, D., Knipper, M., Derst, C., and Fakler, B. (2003) *J. Neurosci.* **23,** 2141–2149
8. Xu, T., Nie, L., Zhang, Y., Mo, J., Feng, W., Wei, D., Petrov, E., Calisto, L. E., Kachar, B., Beisel, K. W., Vazquez, A. E., and Yamoah, E. N. (2007) *J. Biol. Chem.* **282,** 23899–23909
9. Diaz, R. C., Vazquez, A. E., Dou, H., Wei, D., Cardell, E. L., Lingrel, J., Shull, G. E., Doyle, K. J., and Yamoah, E. N. (2007) *J. Assoc. Res. Otolaryngol.* **8,** 422–434
10. Beisel, K. W., Rocha-Sanchez, S. M., Morris, K. A., Nie, L., Feng, F., Kachar, B., Yamoah, E. N., and Fritzsch, B. (2005) *J. Neurosci.* **25,** 9285–9293
11. Hudspeth, A. J. (1989) *Nature* **341,** 397–404
12. Davis, H. (1972) *Ann. Otol. Rhinol. Laryngol.* **81,** 750–751
13. Jentsch, T. J., Steinmeyer, K., and Schwarz, G. (1990) *Nature* **348,** 510–514
14. Wangemann, P. (2002) *Hear Res.* **165,** 1–9
15. Kharkovets, T., Dedek, K., Maier, H., Schweizer, M., Khimich, D., Nouvian, R., Vardanyan, V., Leuwer, R., Moser, T., and Jentsch, T. J. (2006) *EMBO J.* **25,** 642–652
16. Coucke, P., Van Camp, G., Djoyodiharjo, B., Smith, S. D., Frants, R. R., Padberg, G. W., Darby, J. K., Huizing, E. H., Cremers, C. W., Kimberling, W. J., *et al.* (1994) *N. Engl. J. Med.* **331,** 425–431
17. Van Camp, G., Coucke, P. J., Kunst, H., Schatteman, I., Van Velzen, D., Marres, H., van Ewijk, M., Declau, F., Van Hauwe, P., Meyers, J., Kenyon, J., Smith, S. D., Smith, R. J., Djelantik, B., Cremers, C. W., Van de

Heyning, P. H., and Willems, P. J. (1997) *Genomics* **41,** 70–74
18. Mencía, A., González-Nieto, D., Modamio-Høybjør, S., Etxeberría, A., Aránguez, G., Salvador, N., Del Castillo, I., Villarroel, A., Moreno, F., Barrio, L., and Moreno-Pelayo, M. A. (2008) *Hum. Genet.* **123,** 41–53
19. Schwake, M., Pusch, M., Kharkovets, T., and Jentsch, T. J. (2000) *J. Biol. Chem.* **275,** 13343–13348
20. MacKinnon, R. (1991) *Nature* **350,** 232–235
21. Tinker, A., Jan, Y. N., and Jan, L. Y. (1996) *Cell* **87,** 857–868
22. Chouabe, C., Neyroud, N., Guicheney, P., Lazdunski, M., Romey, G., and Barhanin, J. (1997) *EMBO J.* **16,** 5472–5479
23. Su, C. C., Yang, J. J., Shieh, J. C., Su, M. C., and Li, S. Y. (2007) *Audiol. Neurootol.* **12,** 20–26
24. Margeta-Mitrovic, M., Jan, Y. N., and Jan, L. Y. (2000) *Neuron* **27,** 97–106
25. Talebizadeh, Z., Kelley, P. M., Askew, J. W., Beisel, K. W., and Smith, S. D. (1999) *Hum. Mutat.* **14,** 493–501
26. Topsakal, V., Pennings, R. J., te Brinke, H., Hamel, B., Huygen, P. L., Kremer, H., and Cremers, C. W. (2005) *Otol. Neurotol.* **26,** 52–58
27. Campbell, C. A., Della Santina, C. C., Meyer, N. C., Smith, N. B., Myrie, O. A., Stone, E. M., Fukushima, K., Califano, J., Carey, J. P., Hansen, M. R., Gantz, B. J., Minor, L. B., and Smith, R. J. (2010) *Am. J. Med. Genet. A* **152A,** 67–74
28. Lv, P., Wei, D., and Yamoah, E. N. (2010) *J. Biol. Chem.* **285,** 34699–35707
29. Abbott, G. W., and Goldstein, S. A. (2002) *FASEB J.* **16,** 390–400
30. Abbott, G. W., Sesti, F., Splawski, I., Buck, M. E., Lehmann, M. H., Timothy, K. W., Keating, M. T., and Goldstein, S. A. (1999) *Cell* **97,** 175–187
31. Ohyama, H., Kajita, H., Omori, K., Takumi, T., Hiramoto, N., Iwasaka, T., and Matsuda, H. (2001) *Pflugers Arch.* **442,** 329–335
32. Ehrlich, J. R., Pourrier, M., Weerapura, M., Ethier, N., Marmabachi, A. M., Hébert, T. E., and Nattel, S. (2004) *J. Biol. Chem.* **279,** 1233–1241
33. Wu, T., Lv, P., Kim, H. J., Yamoah, E. N., and Nuttall, A. L. (2010) *J. Neurophysiol.* **103,** 1969–1977
34. Cazals, Y. (2000) *Prog. Neurobiol.* **62,** 583–631
35. Guitton, M. J., Caston, J., Ruel, J., Johnson, R. M., Pujol, R., and Puel, J. L. (2003) *J. Neurosci.* **23,** 3944–3952
36. Ruel, J., Chabbert, C., Nouvian, R., Bendris, R., Eybalin, M., Leger, C. L., Bourien, J., Mersel, M., and Puel, J. L. (2008) *J. Neurosci.* **28,** 7313–7323
37. Kakehata, S., and Santos-Sacchi, J. (1996) *J. Neurosci.* **16,** 4881–4889
38. Lue, A. J., and Brownell, W. E. (1999) *Hear Res.* **135,** 163–168
39. Hallworth, R. (1997) *Hear Res.* **114,** 204–212
40. Coucke, P. J., Van Hauwe, P., Kelley, P. M., Kunst, H., Schatteman, I., Van Velzen, D., Meyers, J., Ensink, R. J., Verstreken, M., Declau, F., Marres, H., Kastury, K., Bhasin, S., McGuirt, W. T., Smith, R. J., Cremers, C. W., Van de Heyning, P., Willems, P. J., Smith, S. D., and Van Camp, G. (1999) *Hum. Mol. Genet.* **8,** 1321–1328
41. Akita, J., Abe, S., Shinkawa, H., Kimberling, W. J., and Usami, S. (2001) *J. Hum. Genet.* **46,** 355–361
42. Van Hauwe, P., Coucke, P. J., Ensink, R. J., Huygen, P., Cremers, C. W., and Van Camp, G. (2000) *Am. J. Med. Genet.* **93,** 184–187
43. Kamada, F., Kure, S., Kudo, T., Suzuki, Y., Oshima, T., Ichinohe, A., Kojima, K., Niihori, T., Kanno, J., Narumi, Y., Narisawa, A., Kato, K., Aoki, Y., Ikeda, K., Kobayashi, T., and Matsubara, Y. (2006) *J. Hum. Genet.* **51,** 455–460